Surfactants-assisted preparation of BiVO4 with novel morphologies via microwave method and CdS decoration for enhanced photocatalytic properties

Surfactants-assisted preparation of $BiVO_4$ with novel morphologies via microwave method and CdS decoration for enhanced photocatalytic properties

Zhansheng Wu[a,b*], Yongtao Xue[a], Xiufang He[a], Yunfeng Li[b], Zhilin Wu[c], Giancarlo Cravotto[c,d]

[a.] School of Chemistry and Chemical Engineering, Key Laboratory for Green Processing of Chemical Engineering of Xinjiang Bingtuan, Shihezi University, Shihezi 832003, P.R. China

[b.] School of Environmental and Chemical Engineering, Xi'an Polytechnic University, Xi'an 710048, P.R.China;

[c.] Department of Drug Science and Technology, University of Turin, Turin, 10125, Italy.

[d.] Sechenov First Moscow State Medical University, Center of Bioanalytical Research and Molecular Design, Moscow, Russia.

Corresponding author: Zhansheng Wu, Shihezi University, Shihezi 832003, P.R. China.

Tel: 86993-2055015, Fax: 86993-2057270. E-mail address: wuzhans@126.com

Graphic abstract

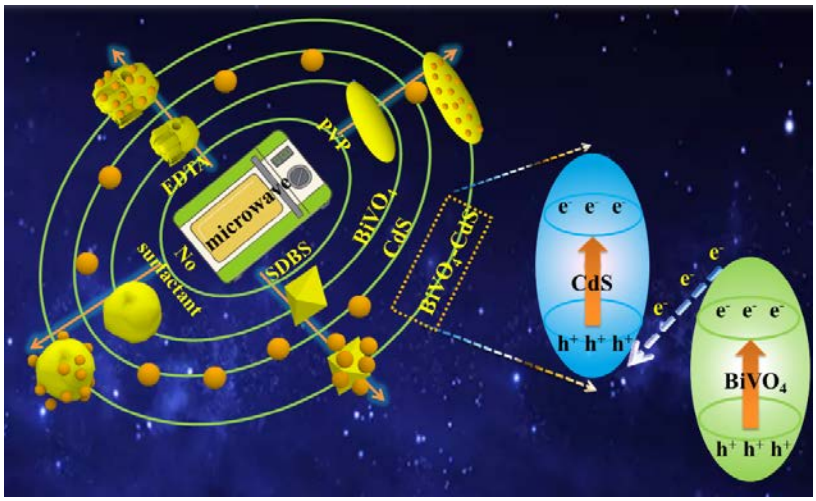

Highlights

1. $BiOV_4$ analogues with different morphologies were prepared using microwave-assisted methods.

2. The mechanisms of regulated morphology and energy-band position for $BiOV_4$, upon treatment with a range of surfactants, have been studied.

3. Increased photocatalytic activity was observed for CdS-decorated $BiOV_4$.

4. A possible Z-scheme mechanism for photodegradation has been proposed

Abstract: The development of a highly efficient and rapid method for the accurate preparation of photocatalysts with novel morphologies is a hot research topic. The different morphologies of $BiVO_4$ was prepared using surfactants-assisted microwave method, and demonstrated irregular (no surfactant), octahedral (sodium dodecyl benzene sulfonate), olive-like (polyvinylpyrrolidone) and hollow structures (ethylenediaminetetraacetic acid), respectively. The $BiVO_4$-CdS were synthesized using the chemical-bath-deposition method with different morphologies of $BiVO_4$as the substrates. The hollow structure of $BiVO_4$displayed the highest photocatalytic performance. Moreover, the photodegradation rates of the hollow structure $BiVO_4$-CdS on tetracycline hydrochloride and ciprofloxacin were about 1.8 and 1.5 times higher than the corresponding $BiVO_4$, indicating that the Z-scheme heterojunction can improve the photogenerated electron pairs separation efficiency. Furthermore, the regulation mechanism of morphology and energy-band position, as produced using the surfactants, has also been thoroughly investigated in this work, which provides a novel insight into the efficient and rapid preparation of photocatalysts with special morphology and high performance.

Keywords: microwave, surfactants, $BiVO_4$-CdS, Z-scheme, photodegradation

1. Introduction

In recent years, bismuth vanadate ($BiVO_4$) has been widely applied in the photodegradation of pollutants because of its relatively high stability and photocatalytic efficiency [1, 2]. At present, $BiVO_4$ is commonly prepared via the sol-gel and hydrothermal methods [3, 4]. However, these synthetic procedures usually require high temperature and pressure conditions, which are not suitable for sustainable development. In other words, the development of new efficient methods for the preparation of $BiVO_4$ is an urgent requirement. In recent years, microwave-assisted synthetic methods have received ever greater amounts of attention [5]. Microwave heating can achieve the simultaneous heating of the surface and interior of the reactants, which can speed up reaction rates and increase yields [6, 7]. Wang et al., have reported the microwave-assisted preparation of Tb^{3+}-$BiVO_4$, and the results showed that the rate of the photodegradation of methylene blue by composites reached 99.9% after irradiation for 120 min under visible light [8]. Liu et al., have synthesized sandwich-like $BiVO_4$ sheets with high visible-light photocatalytic activity using a facile and rapid microwave-assisted method [9]. Therefore, it is feasible to prepare high performance $BiVO_4$ via the microwave-assisted method.

Although $BiVO_4$ can be prepared using the microwave-assisted method, the shape, size and energy-band structure of $BiVO_4$ still require further improvement. Fortunately, surfactants can not only control the size of $BiVO_4$, but also regulate the position of the energy-band structure to improve photocatalytic performance [10]. Wei et al., have successfully prepared $BiVO_4$ nanosheets using a sodium dodecyl benzene sulfonate (SDBS)-assisted hydrothermal method [11]. Ye et al., have used polyvinylpyrrolidone (PVP) as a soft template for the synthesis of pumpkin-like microstructure $BiVO_4$ with remarkable photoactivity [12]. Zhao et al., have synthesized nanostructured shuriken-like $BiVO_4$ using a solvothermal process and ethylenediamine tetraacetic acid disodium (EDTA) as the structure-directing agent [13]. However, to the best of our knowledge, the use of the microwave-assisted method together with a number of surfactants to regulate the structure and morphology of

$BiVO_4$ has not yet been reported. Furthermore, the intrinsic effects of that the surfactants have on the preparation of $BiVO_4$ have also not been studied in depth. Consequently, a study of the role that surfactants have on the microwave-assisted preparation of $BiVO_4$ is still essential.

In spite of this, the catalytic efficiency of single $BiVO_4$ is too low for practical applications. Constructing the Z-scheme photocatalytic system with $BiVO_4$ and CdS has previously been investigated as a promising way to improve photocatalytic efficiency [14]. Selvam et al., have used $BiVO_4$/rGO/CdS to achieve the efficient photodegradation of isoniazid and 1, 4-dioxane [15]. Wei et al., have constructed Z-scheme photocatalysts of $BiVO_4$/CdS, which exhibited enhanced photocatalytic activity for CO_2 reduction [16]. Therefore, the method with which $BiVO_4$ is prepared by microwave methods and surfactants, and then how the Z-scheme photocatalyst is formed with CdS are the keys to achieving efficient photocatalysis.

This paper describes the successful preparation of $BiVO_4$, with different structures and morphologies, via a microwave-assisted method using different surfactants (SDBS, PVP, EDTA). Afterwards, the $BiVO_4$-CdS Z-scheme photocatalytic system was synthesized using the chemical-bath-deposition (CBD) method. The effect of the different surfactants on the morphology and energy-band structure of $BiVO_4$ has been deeply investigated, and the photocatalytic mechanism has also been analysed. Our current work is expected to offer a novel insight into this facile method for the synthesis of a high efficiency photocatalyst and provide a theoretical basis for the effect of several surfactants on the photocatalyst.

2. Materials and methods

2.1 Materials

Bismuth (III) nitrate pentahydrate and ammonium metavanadate were purchased from Adamas. SDBS, PVP, EDTA and thiourea were purchased from Sinopharm Chemical Reagent Co., Ltd. China. Cadmium acetate dihydrate (Shanghai Maclean Biochemical Co., Ltd. China), and ITO glass (South China Xiangcheng Technology Co., Ltd. China) were used.

2.2 Photocatalyst preparation

2.2.1 Synthesis of $BiVO_4$

The monoclinic $BiVO_4$ sample was synthesized via a microwave-assisted method (Scheme 1). Typically, 5 mmol $Bi(NO_3)_3 \cdot 5H_2O$ was dissolved in 50 mL of 2 mol/L HNO_3 solution and stirred uniformly, and then the surfactants (0.2 g SDBS, 1.5 g PVP, 1.3 g EDTA) were added. Subsequently, 5 mmol NH_4VO_3 was added into the mixed solution. After being stirred for 1 h, the solution was transferred into an atmospheric-pressure microwave reactor at the temperature of 100 °C operating at a speed of 2000 r/min (MCR-3, Shanghai Kehao Instrument Equipment Co., Ltd. China), which was maintained for 3 h. The yellow powder was washed with acetone, deionized water and absolute alcohol more than 3 times, and then dried at 80 °C in a vacuum oven for overnight. The samples are expressed as S-$BiVO_4$, P-$BiVO_4$ and E-$BiVO_4$, respectively. $BiVO_4$ was obtained without the addition of a surfactant.

2.2.2 Synthesis of $BiVO_4$-CdS

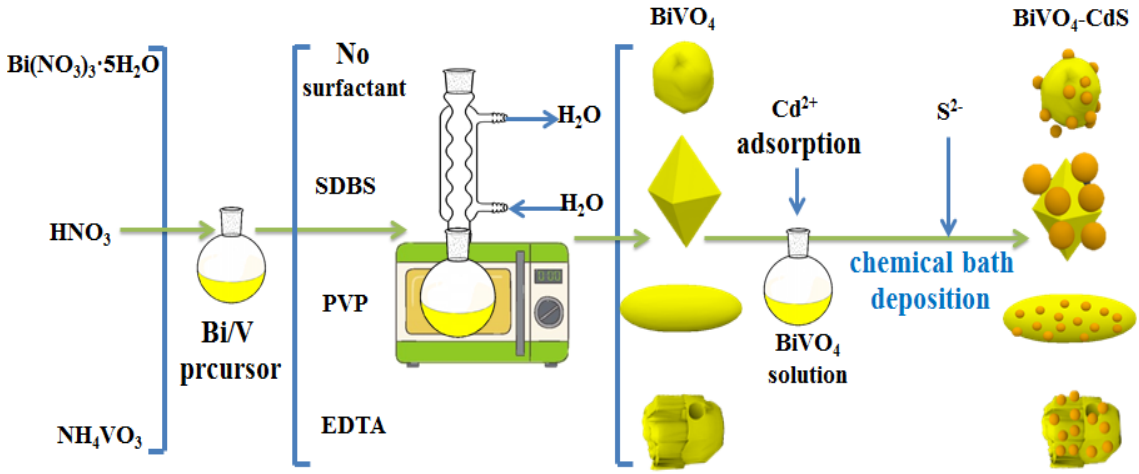

Scheme 1 Schematic illustration for the formation of $BiVO_4$- CdS photocatalysts

The $BiVO_4$-CdS composite was fabricated using the CBD method. 40 mg of $BiVO_4$ was added to 40 mL deionized water containing 1.48 g Cd $(CH_3COO)_2 \cdot 2H_2O$. The solution was then stirred for

30 min to achieve the preferential absorption of Cd^{2+} onto the surface of $BiVO_4$. Subsequently, 0.8 g CH_4N_2S was added to the above solution and maintained at 80 °C for 30 min. The precipitate was washed with deionized water several times and dried at 60 °C in a vacuum oven for 10 h. The resulting samples were named: $BiVO_4$-CdS, S-$BiVO_4$-CdS, P-$BiVO_4$-CdS, E-$BiVO_4$-CdS.

2.3. Characterisation

The crystallographic properties of the samples were characterised using XRD patterns (Rigaku Corporation, Tokyo, Japan). XPS spectra, XPS valence band (VB-XPS) (AMICUS/ESCA 3400, Japan) and SEM (SU8010, Japan) were used to evaluate the structure and morphology of the samples. Diffuse reflectance spectra (Hitachi UV-4100, Japan) and photoluminescence spectra (PL) (FLsp920, England) were used to characterise optical performance. Raman spectra were obtained on a Raman microscope (LabRAM HR800, France) with an excitation wavelength of 532 nm. The active species were investigated in an electronic paramagnetic resonance spectrometer (JES FA200, Japan) using DMPO (5, 5-dimethyl-1-pyrroline N-oxide) as the free-radical trapping agent. Transient photocurrent response spectra were recorded in an electrochemical system (CHI-760D, China) including a Pt electrode, an Ag/AgCl electrode and an ITO glass (2 cm^2) as a working electrode. A 0.1 M aqueous Na_2SO_4 solution was selected as the electrolyte. The electrochemical impedance spectra (EIS) measurements were measured in the presence of a $Fe(CN)_6^{3-/4-}$ solution.

2.4 Photocatalytic activity measurements

The photocatalytic activity of the $BiVO_4$-CdS photocatalyst was evaluated using the photodegradation of either tetracycline hydrochloride (20 mg/L, TCH) or ciprofloxacin (10 mg/L, CIP) under simulated sunlight irradiation (AM1.5 cut-off filter). Before the light irradiation, 20 mg of the photocatalyst and 50 mL of either the TCH or CIP solutions was stirred for 0.5 h in the dark. The concentrations of TCH and CIP were measured using a UV-5100 UV-vis spectrophotometer at 357 nm and 277 nm.

3. Results and discussion

3.1 Structure and morphology characteristics

The crystal structure of the prepared photocatalysts was determined by XRD. In Fig.1a, it can be seen that all the $BiVO_4$ presented similar characteristic peaks at 18.63°, 29.92°, 30.53°, 53.32°, which correspond to the (011), (121), (040), (161) crystal planes of monoclinic $BiVO_4$, respectively (JCPDS NO. 14-0688) [17]. Furthermore, the crystal structure and composition of $BiVO_4$ did not change noticeably and no other impurities were observed in the presence of the different surfactants, indicating that these surfactants did not affect the crystal structure of $BiVO_4$. As shown in Fig.1b, pure CdS showed four characteristic peaks at 25.0°, 26.5°, 28.3°, and 43.9°, which correspond to the (100), (002), (101) and (110) crystal planes of hexagonal CdS, respectively (JCPDS NO. 41-1049) [18]. Good coexistence between $BiVO_4$ and CdS was observed for the $BiVO_4$-CdS composites, suggesting that CdS had successfully entered the $BiVO_4$ systems. However, the characteristic peaks of CdS showed low intensity in $BiVO_4$-CdS composites. This might be attributed to the low content of CdS. The XRD results also indicated that CdS did not affect the crystal structure of $BiVO_4$.

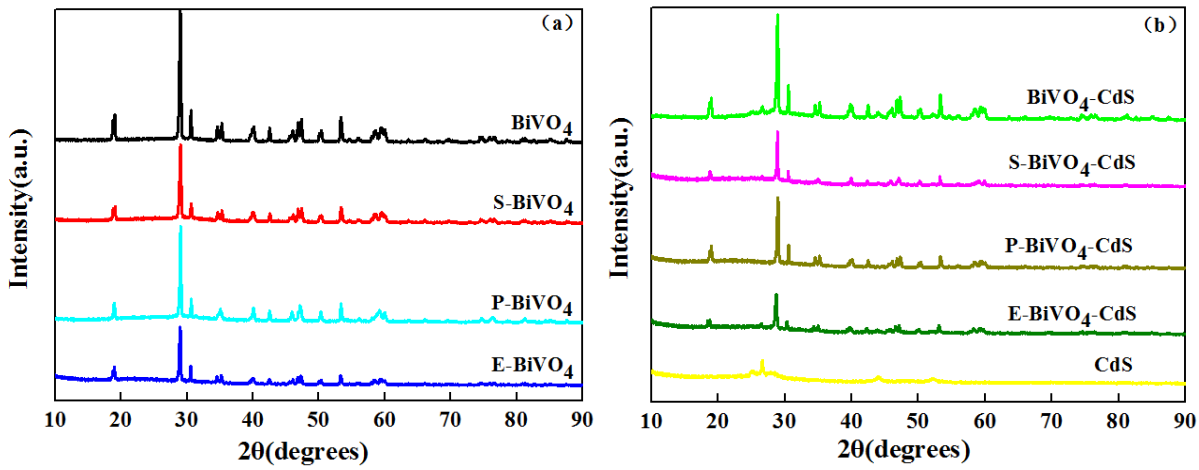

Fig.1. XRD patterns of prepared $BiVO_4$ (a) and $BiVO_4$-CdS, CdS (b)

Fig.S1 displays the Raman spectra for the detection of the presence of CdS in the composites. In Fig.S1a, it can be observed that $BiVO_4$ shows five peaks, which are located at around 127.5, 212.8, 328.3, 367.45, 831.2 cm^{-1}. These can be attributed to the monoclinic phase of $BiVO_4$ [19]. The $BiVO_4$ Raman spectra underwent no significant changes in the presence of different surfactants, indicating

that these surfactants did not alter the crystal structure of $BiVO_4$. For CdS, the two peaks at 303.4 and 605.4 cm^{-1} can be ascribed to the first-order longitudinal (1-LO) and second-order longitudinal (2-LO) of CdS [20]. In addition, the characteristic CdS peaks appeared in all $BiVO_4$-CdS. The $BiVO_4$ Raman spectra show no obvious change in $BiVO_4$-CdS, suggesting that the $BiVO_4$-CdS composite had been prepared successfully.

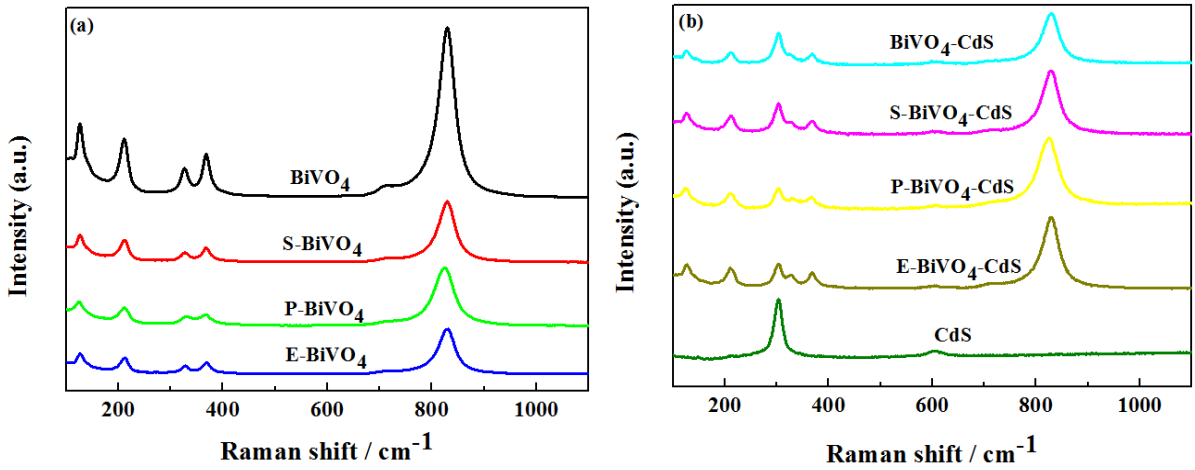

Fig.S1 Raman spectra of $BiVO_4$, CdS and $BiVO_4$-CdS

XPS analyses were conducted to further confirm the chemical status of the prepared samples. As can be seen in Fig.S2a, all the $BiVO_4$-CdS survey spectra were composed of Bi, V, O, Cd and S, compared with pure $BiVO_4$ and CdS, indicating that the $BiVO_4$-CdS composites were successfully constructed. As illustrated in Fig.S2b-d, the characteristic orbitals of Bi $4f_{7/2}$, Bi $4f_{5/2}$, V $2p_{3/2}$, V $2p_{1/2}$, O 1s from $BiVO_4$ appeared at 159.3, 164.5, 516.8, 524.5, and 529.8 eV, respectively, suggesting that all the $BiVO_4$ were successfully synthesized, and the surfactants had no significant effect on the chemical composition of $BiVO_4$ [21]. In addition, the intensities of Bi 4f, V 2p and O 1s in $BiVO_4$-CdS were much lower than in $BiVO_4$. This was ascribed to the fact that CdS was successfully deposited onto the surface of $BiVO_4$. As seen in Fig.S2e-f, the CdS peaks at 405.1 and 411.8 eV correspond to Cd^{2+}, while the peaks positioned at 161.4 and 162.7 eV were assigned to S^{2-} [22]. Moreover, $BiVO_4$-CdS displayed similar Cd 3d and S 2p peaks to CdS, which further confirms that the $BiVO_4$-CdS composites were successfully assembled.

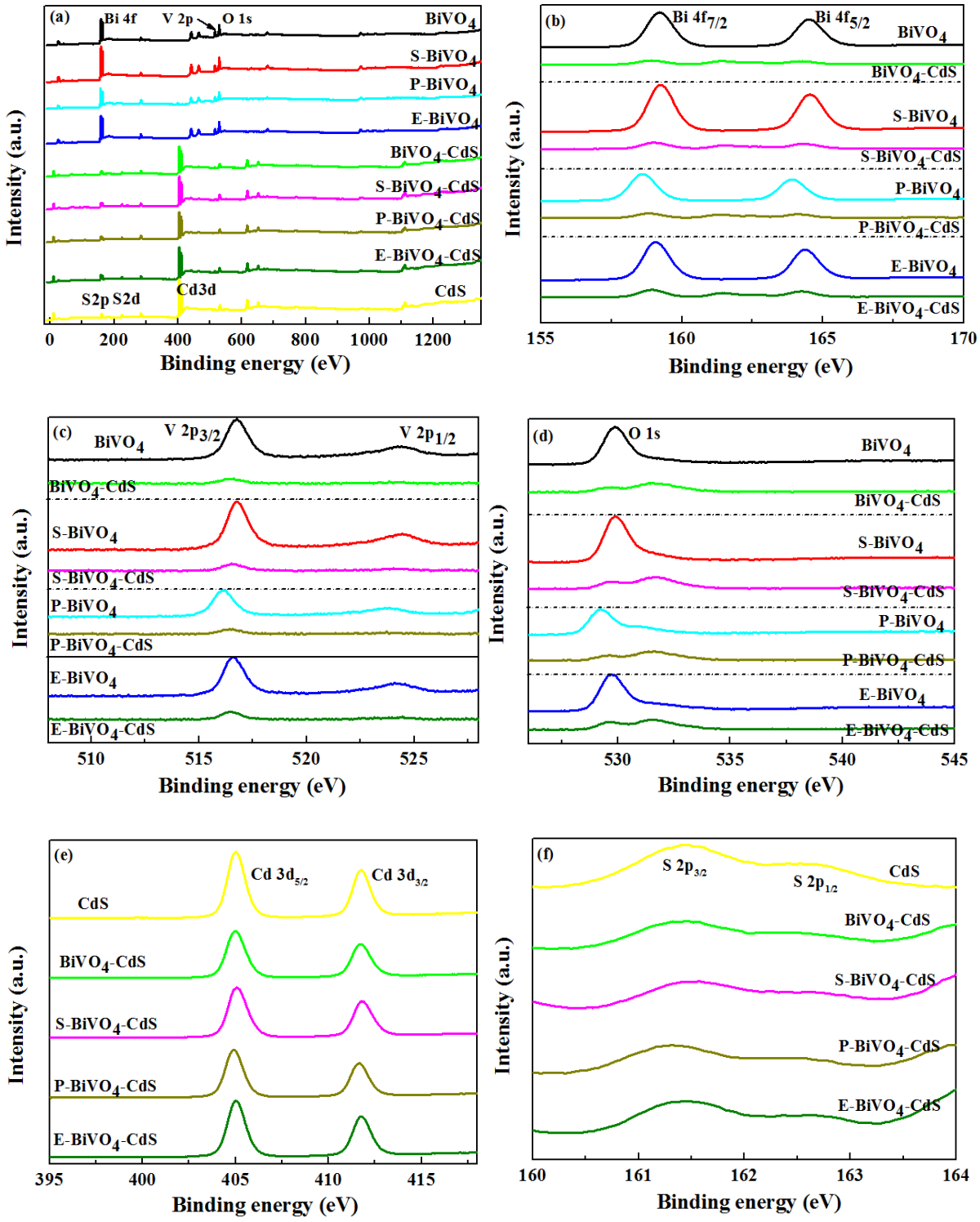

Fig.S2. XPS spectra of $BiVO_4$, $BiVO_4$-CdS and CdS samples; (a) survey spectrum, (b) Bi 4f, (c) V 2p, (d) O 1s, (e) Cd 3d, (f) S 2p

SEM characterisation was used to study the morphological structure of the samples. As shown in Fig. 2a, pure CdS displayed relatively uniform microspheres with diameters of 300 nm. In Fig. 2b, it can be seen that $BiVO_4$ was present as irregular polyhedrons with smooth surfaces. After depositing CdS nanoparticles, some small particles appeared on the surface of $BiVO_4$-CdS (Fig. 2c). An examination of Fig. 2c and the EDS mapping images of $BiVO_4$-CdS prove that CdS was successfully deposited on the surface of $BiVO_4$. In addition, S-$BiVO_4$ showed an octahedral structure with a diameter of 350 nm (Fig. 2d), and P-$BiVO_4$ had an almost olive-like structure with a length of about 2.2 μm (Fig. 2f) E-$BiVO_4$ displayed a porous irregular polyhedron structure with a diameter of about 250 nm (Fig. 2h). Furthermore, the CdS particles were clearly present on the surfaces of S-$BiVO_4$ (Fig. 2e), P-$BiVO_4$ (Fig. 2g) and E-$BiVO_4$ (Fig. 2i), indicating that all the $BiVO_4$-CdS were successfully prepared. Notably, the presence of surfactants had a great effect on the morphology and size of $BiVO_4$, and might further affect the photodegradation performance of $BiVO_4$.

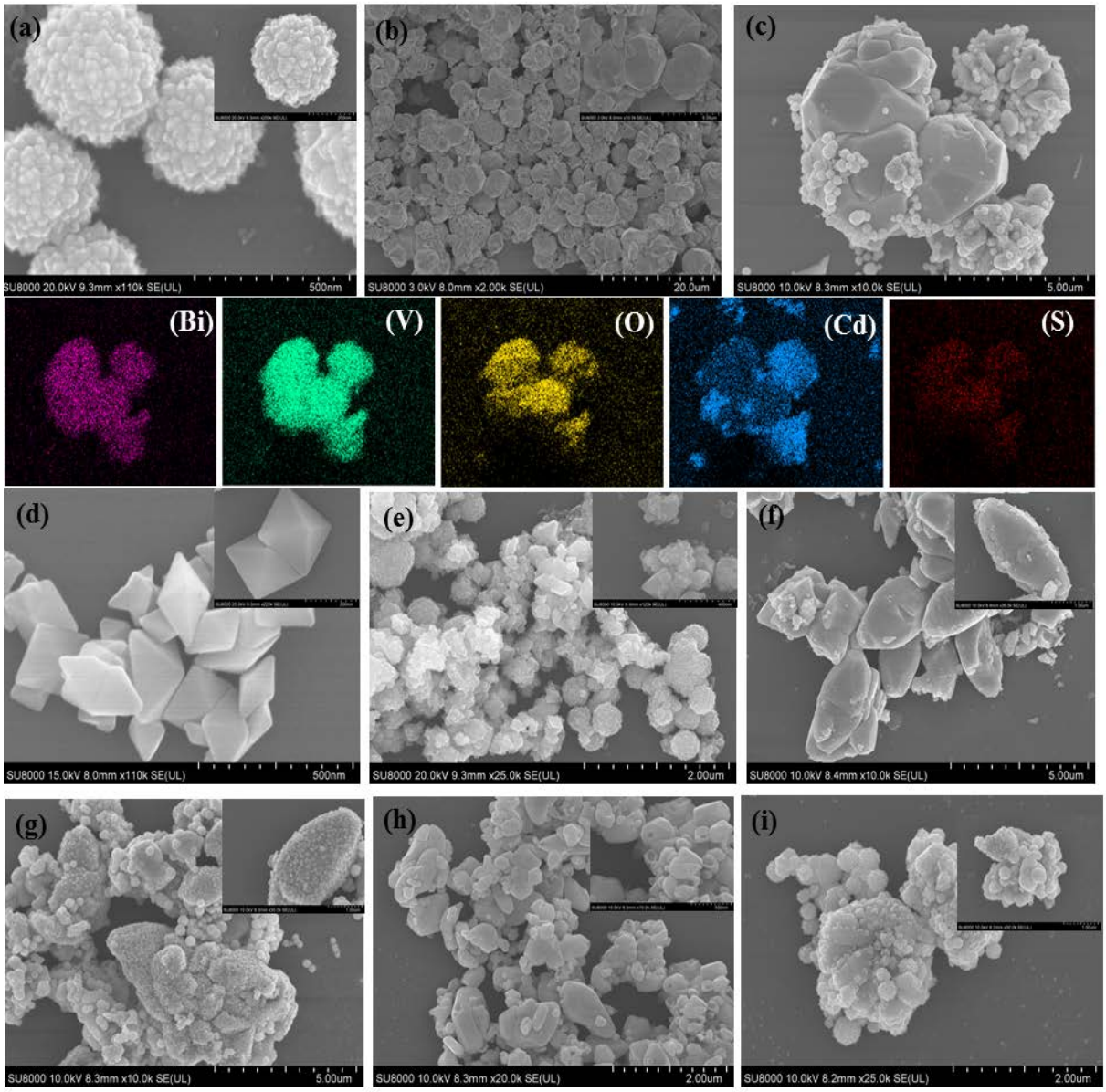

Fig.2. SEM patterns of the samples (a) CdS, (b) $BiVO_4$, (c) $BiVO_4$-CdS, (d) S-$BiVO_4$, (e) S-$BiVO_4$-CdS, (f) P-$BiVO_4$, (g) P-$BiVO_4$-CdS, (h) E-$BiVO_4$, (i) E-$BiVO_4$-CdS, EDS mapping images of $BiVO_4$-CdS

The effect of surfactants on the morphology of $BiVO_4$ was therefore thoroughly studied, and the results are shown in Fig.3. In the absence of a surfactant, Bi^{3+} and VO_3^- can easily diffuse and contact in solution and then nucleate meaning that $BiVO_4$ can be formed quickly under microwave conditions. The final particle size is large and the shape is irregular [23]. SDBS is an anionic surfactant with

selective adsorption on the plane of the nuclei, which can be used to prepare nanoparticles of specific shape. In the present case, the SDBS may be adsorbed onto the (010) plane of the $BiVO_4$ nuclei and affect their growth [24]. Thus, it is possible that the formed nanomaterials will not grow along the (040) plane due to the inhibition of SDBS, resulting in the extrusion of the crystal face and the formation of the octahedral structure of $BiVO_4$. PVP, as a nonionic polymer compound, is often used as a surfactant and capping agent. Additionally, the pyrrole moiety of PVP has a negative charge, making the formation of Bi^{3+}- PVP complex [11]. It can be speculated that PVP acts as a "soft" template, and the complex can be dissolved, to then recrystallize, self-assemble and form the olive-like structure of $BiVO_4$. EDTA is an important complexing agent that can be used to control the morphology of nanomaterials. In the presence of EDTA, Bi^{3+} can be combined with EDTA and VO_3^- due to the excess of Bi^{3+} compared with EDTA. (do you mean more easily combined? It is not clear where the comparison is) $BiVO_4$ can be formed through the dissolution-recrystallization process: (Bi^{3+}-EDTA)+VO^{3-}+H_2O→Bi^{3+}+$EDTA^-$+VO^{3-}+H_2O→$BiVO_4$+EDTA+$2H^+$) [25].

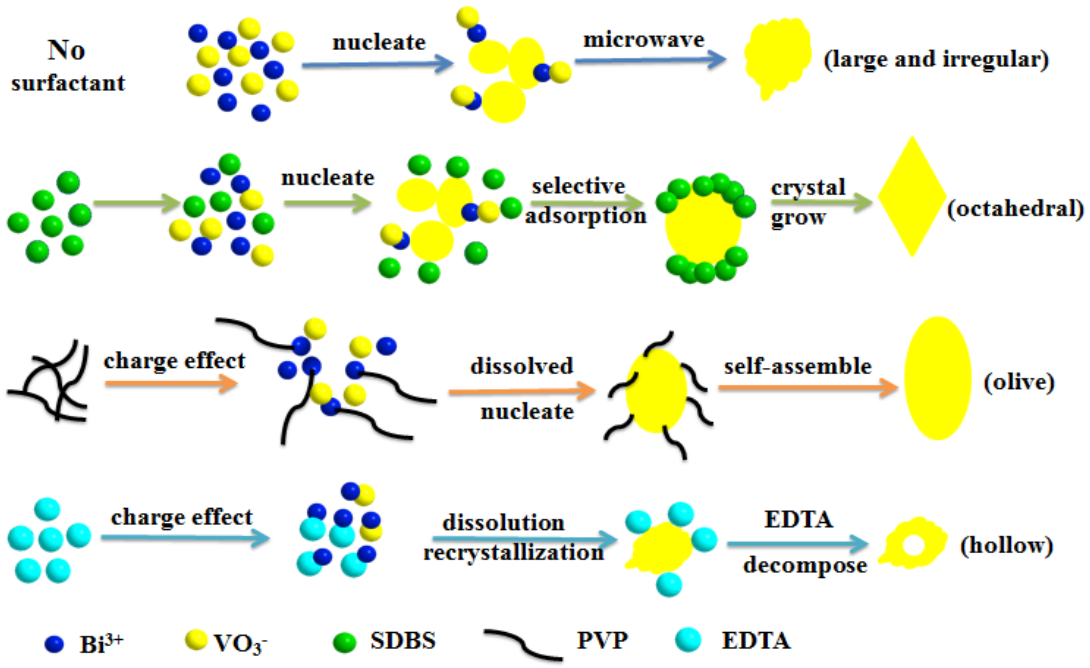

Fig.3. Schematic illustration for formation of the $BiVO_4$ morphology

Moreover, microwave pyrolysis is a rapid heating process in which heat transfers from the inside to the surface via microwave radiation. It is therefore possible that EDTA may decompose into CO_2 and H_2O, and then the gas will congregate at the nuclei of $BiVO_4$ to form the hollow structure [26]. Based on the above analysis, the surfactants have a significant influence on the morphology of $BiVO_4$, which may further affect photocatalytic performance.

3.2 Optical properties

UV-vis diffuse reflectance spectra were performed in order to investigate the light-absorption properties of the samples. As depicted in Fig.S3a, $BiVO_4$ produced an absorption edge at around 550 nm that can be assigned to the band gap of $BiVO_4$, which corresponds to about 2.24 eV (Fig.S3a insect). Moreover, the absorption edge of S-$BiVO_4$, P-$BiVO_4$ and E-$BiVO_4$ showed a significant blue shift compared to $BiVO_4$, and the band gaps were calculated to be 2.34, 2.29, 2.37 eV, respectively. An analysis of the SEM results indicates that the blue shift phenomenon may be caused by the quantum size effect [27]. As seen in Fig.S3b, CdS had an absorption edge at 540 nm, and the absorption edge of all $BiVO_4$-CdS displayed a blue shift compared with $BiVO_4$, suggesting that the $BiVO_4$-CdS composites were successfully synthesized and that photocatalytic ability might be improved [28].

Transient-photocurrent spectra and electrochemical-impedance spectra were used to investigate the separation efficiency of the photoelectron-hole pair. As shown in Fig.S3c, the photocurrent of all the samples increased significantly under illumination, as compared with dark conditions, indicating that the sample was able to generate electrons and holes under illumination. In addition, the photocurrent increased in the order: $BiVO_4$ < P-$BiVO_4$ < S-$BiVO_4$ < E-$BiVO_4$ and $BiVO_4$-CdS < P-$BiVO_4$-CdS < S-$BiVO_4$-CdS < E-$BiVO_4$-CdS, suggesting that the surfactant can increase the photogenerated-electron and hole-separation efficiency of $BiVO_4$ [29]. This is due to the fact that the nanomaterials shorten the distance and time that photogenerated carriers migrate from the interior of the photocatalyst to the surface, as compared with micron-materials. This result is consistent with the

results of the SEM. Moreover, all of the $BiVO_4$-CdS displayed a higher photocurrent than $BiVO_4$. This was assigned to the formation of a heterojunction that promoted the separation of the photoelectron-hole pair [30].

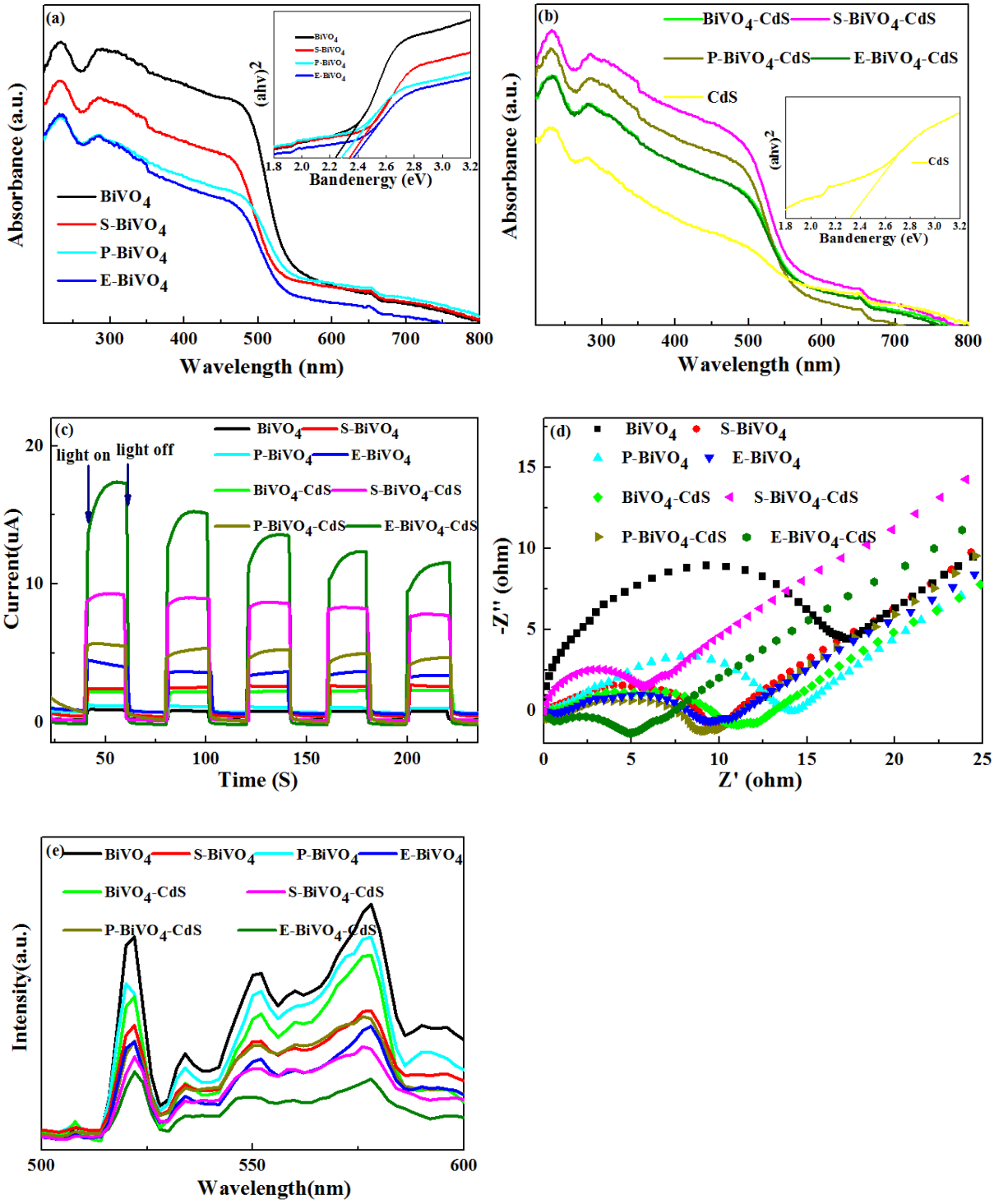

Fig.S3. UV–Vis diffuse reflectance spectra of $BiVO_4$ (a), $BiVO_4$-CdS and CdS (b), transient photocurrent spectra (c), electrochemical impedance spectra (d), PL spectra (e)

As seen in Fig.S3d, a smaller EIS arc radius suggests higher charge mobility and higher photogenerated-electron and hole-separation efficiency. The order of the resistance is therefore in accordance with the results of the transient photocurrent [31]. The PL spectra of the samples are presented in Fig.S3e and it can be seen that $BiVO_4$ had the highest PL signal. By contrast, E-$BiVO_4$-CdS displayed the lowest peak intensity. The results suggest that the recombination rate of the photoelectron-hole pair was inhibited by the combination of $BiVO_4$ and CdS [32]. The electrochemistry and PL results both confirmed that the surfactants and heterojunction provide significant improvements in photoelectron-hole-pair separation and that they might further enhance photocatalytic performance.

3.3 Photocatalytic activity

TCH was chosen as the typical antibiotic contaminant to evaluate the photocatalytic activities of the samples. As showed in Fig. 4a-b, all the samples displayed insignificant adsorption amounts for TCH under dark conditions. Pure $BiVO_4$ displayed the lowest photocatalytic efficiency under simulated sunlight irradiation, which can be ascribed to the fast electron-hole recombination. S-$BiVO_4$, P-$BiVO_4$ and E-$BiVO_4$ demonstrated higher photocatalytic performance than $BiVO_4$, which indicated that the surfactants were able to significantly improve the photocatalytic performance that resulted from the regulation of the morphology and structure of $BiVO_4$ [33]. Furthermore, the degradation of TCH was in accordance with pseudo-first-order kinetics, and the photodegradation rate of all $BiVO_4$-CdS samples was about 1.8-times higher than that of $BiVO_4$ (Fig.S4a-b), indicating that the formation of a heterojunction can improve photocatalytic efficiency. This result was also consistent with those of the transient photocurrent spectra and electrochemical impedance.

CIP was deployed as another target antibiotic contaminant to further evaluate the photocatalytic properties of the sample. As can be observed in Fig. 4c, E-$BiVO_4$ clearly showed higher adsorption than $BiVO_4$, S-$BiVO_4$ and P-$BiVO_4$ under dark conditions, which might be ascribed to the hollow

structure of E-$BiVO_4$. Moreover, S-$BiVO_4$, P-$BiVO_4$ and E-$BiVO_4$ displayed higher photocatalytic activity than $BiVO_4$.

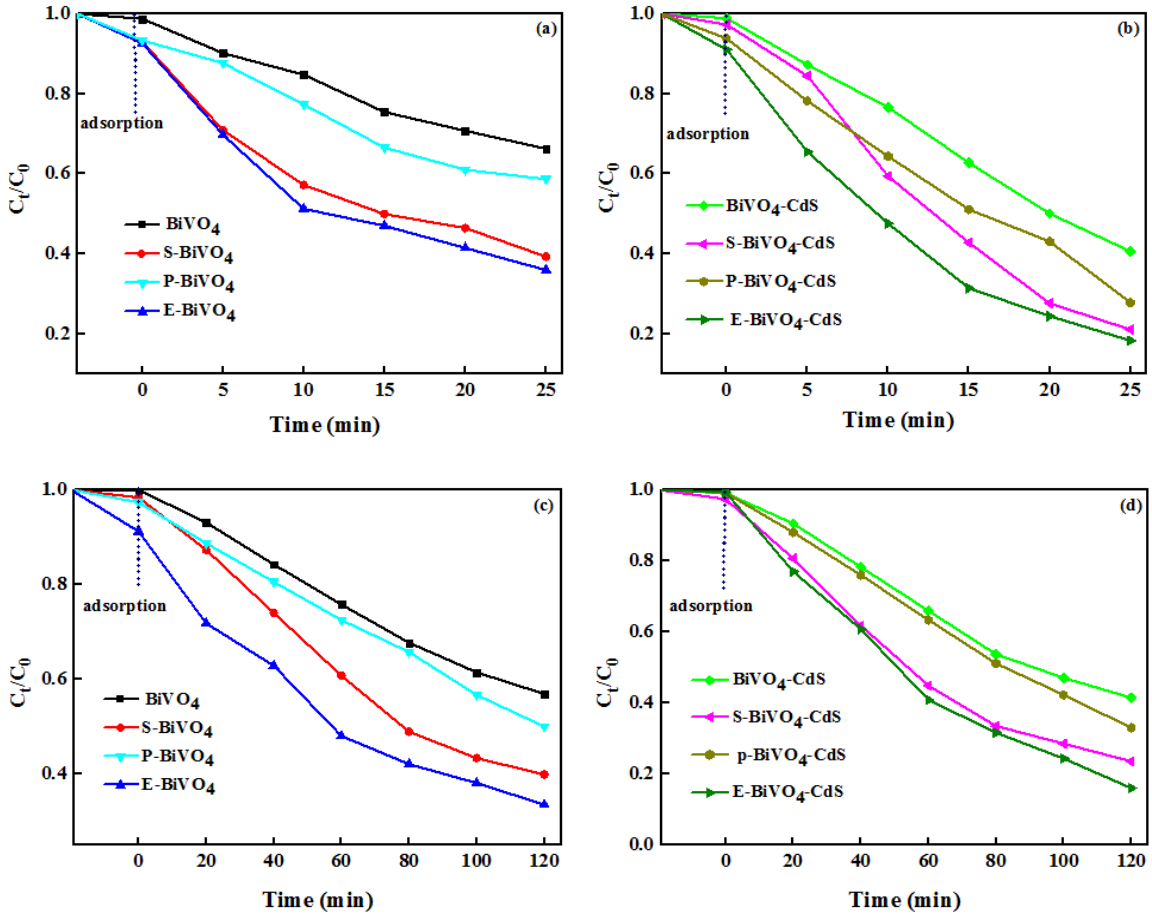

Fig.4. Photocatalytic degradation of TCH (a, b) and CIP (c, d), over samples

As a result, it is further confirmed that the surfactant can significantly improve photocatalytic performance. As shown in Fig. 4d, all the $BiVO_4$-CdS analogues displayed higher photocatalytic activity than $BiVO_4$, and the photodegradation rate of all the $BiVO_4$-CdS samples was about 1.5-times that of the corresponding $BiVO_4$ (Fig.S4c-d). Based on the results of photocatalytic degradation for TCH and CIP, it can be concluded that the surfactant and heterojunction effect can improve photocatalytic efficiency.A comparison of the photocatalytic activity of $BiVO_4$-CdS composites with previously reported similar photocatalyst systems for the photodegradation of TCH and CIP is presented in Table 1.

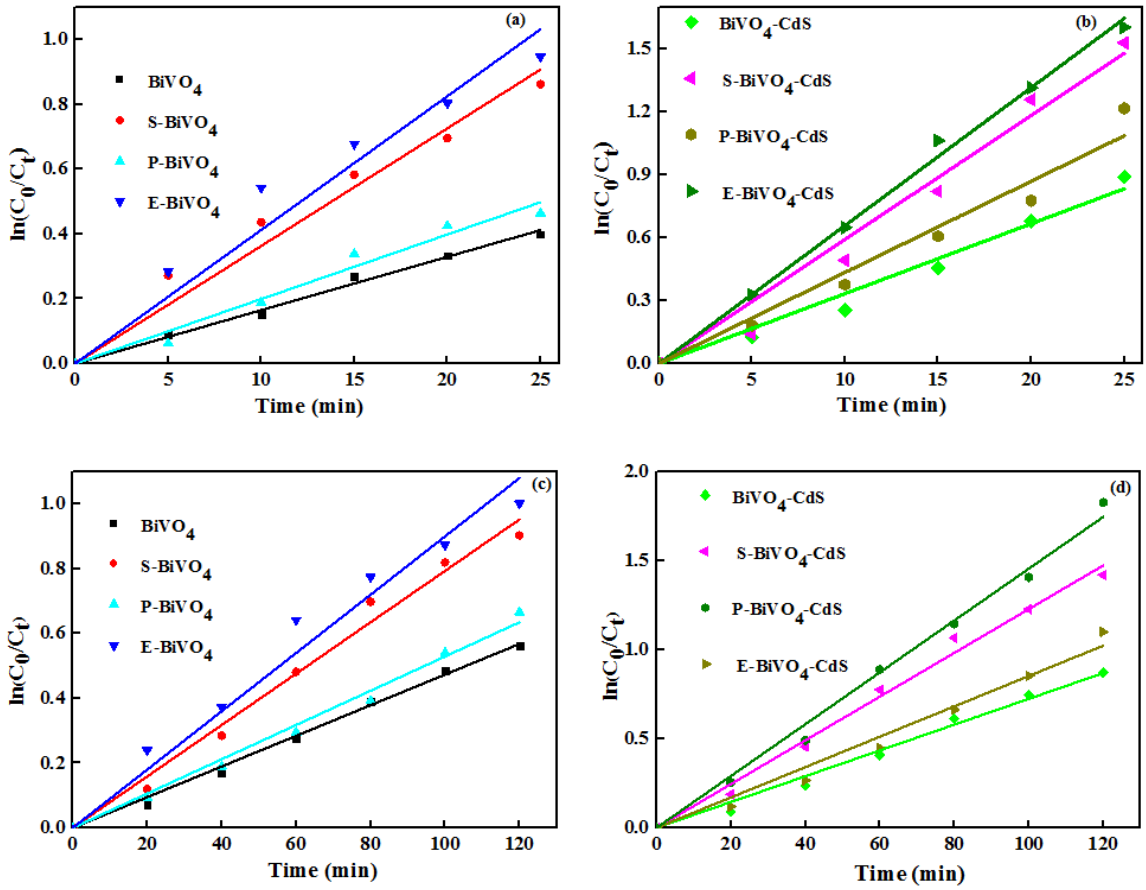

Fig.S4. pseudo-first-order kinetics of TCH (a, b) and CIP (c, d) degradation

As can be seen, E-$BiVO_4$-CdS displayed the highest photocatalytic performance for TCH and CIP, as compared with other similar photocatalysts system. This verifies that $BiVO_4$-CdS composites can not only be prepared quickly and easily, but that they also have great potential applications in TCH and CIP removal from contaminated water.

Table 1 Comparison with other photocatalysts for the degradation of TCH and CIP

Photocatalysts	Quality (mg)	Light source (Power, W)	Concentration (mg/L)	Volume (mL)	Degradation (%); Time	Refs.
E-$BiVO_4$-CdS	20 mg	Xenon lamp 300 W	20 mg/L	50 mL	TCH; 82.1%;25min	This work
Ag-B-Au- $BiVO_4$	10 mg	metal halide lamp 250 W	20 mg/L	50 mL	TCH; 79%;50min	[3]
Ag/Ag_2CO_3/$BiVO_4$	20 mg	Xe lamp 500 W	20 mg/L	50 mL	TCH; 94.9%;150min	[30]
g-C_3N_4/QDs/$BiVO_4$	30 mg	Xenon lamp 250 W	20 mg/L	100 mL	TCH; 73.8%;60min	[34]
E-$BiVO_4$-CdS	20 mg	Xenon lamp 300 W	10 mg/L	50 mL	CIP 84.1%;120min	This work
$BiVO_4$/NGQDS/ g-C_3N_4	50 mg	Xenon lamp 250 W	10 mg/L	100 mL	CIP; 72.4%;120min	[17]
CQDs/BiOBr	30 mg	Xenon lamp 300 W	10 mg/L	100 mL	CIP; 70%;240min	[31]
$Bi_4V_2O_{11}$/CdS	50 mg	Xenon lamp 250 W	10 mg/L	100 mL	CIP; 76.9%;120min	[35]

3.4 Mechanism of photodegradation

In order to further clarify the main active species for TCH and CIP photodegradation, trapping experiments were performed and the results are illustrated in Fig.5a-b. In TCH photodegradation, there was an obvious decrease in the presence of EDTA-2Na for all $BiVO_4$-CdS, which indicates that h^+ played a key role. The addition of IPA and BQ resulted in a slight reduction, demonstrating that •OH and $•O_2^-$ had a weak effect on the photodegradation of TCH. It could be speculated that h^+ was the main active species in all the $BiVO_4$-CdS-promoted photodegradations of TCH. Furthermore, photocatalytic performance in CIP photodegradation rapidly decreased after the addition of BQ, and

decreased slightly after adding IPA and EDTA-2Na with all $BiVO_4$-CdS, indicating that $\bullet O_2^-$ was the main active species for the photodegradation of CIP. ESR spectra were also performed to demonstrate the effect of $\bullet O_2^-$ and •OH, and the results are shown in Fig.5c-d. The characteristic peaks of $\bullet O_2^-$ and •OH were not detected in dark conditions. However, the characteristic O_2^- and •OH peaks were shown to be higher under illumination, and the intensity increased with time. The results further confirm that $\bullet O_2^-$ and •OH were involved in photodegradation, which is consistent with the results of the trapping experiments. In addition, the intensity of $\bullet O_2^-$ and •OH increases in the order: $BiVO_4$-CdS < P-$BiVO_4$-CdS < S-$BiVO_4$-CdS < E-$BiVO_4$-CdS, indicating that E-$BiVO_4$-CdS can promote the separation of photoelectron holes and thus produce more reactive groups for photocatalytic TCH and CIP removal than other $BiVO_4$-CdS. These results provide convincing proof that E-$BiVO_4$-CdS has the highest photocatalytic performance [36].

In order to further understand the difference in the amount of $\bullet O_2^-$ and •OH produced by $BiVO_4$-CdS, the valence-band levels (VB) of $BiVO_4$ and CdS were acquired from VB-XPS (Fig.5e-f). The VB maximum values for $BiVO_4$, S-$BiVO_4$, P-$BiVO_4$, E-$BiVO_4$ and CdS were revealed to be 2.43, 2.61, 2.52, 2.67 and 1.62 eV, respectively. Based on the results of UV-Vis and VB-XPS, the conduction-band (CB) values were calculated to be 0.19, 0.27, 0.23, 0.30 and -0.7 eV, respectively [37]. Additionally, the band structures of $BiVO_4$ and CdS are demonstrated in Fig.S5. Importantly, the surfactants can change the CB and VB positions of $BiVO_4$, which may be better matched with CdS to produce more $\bullet O_2^-$ and •OH.

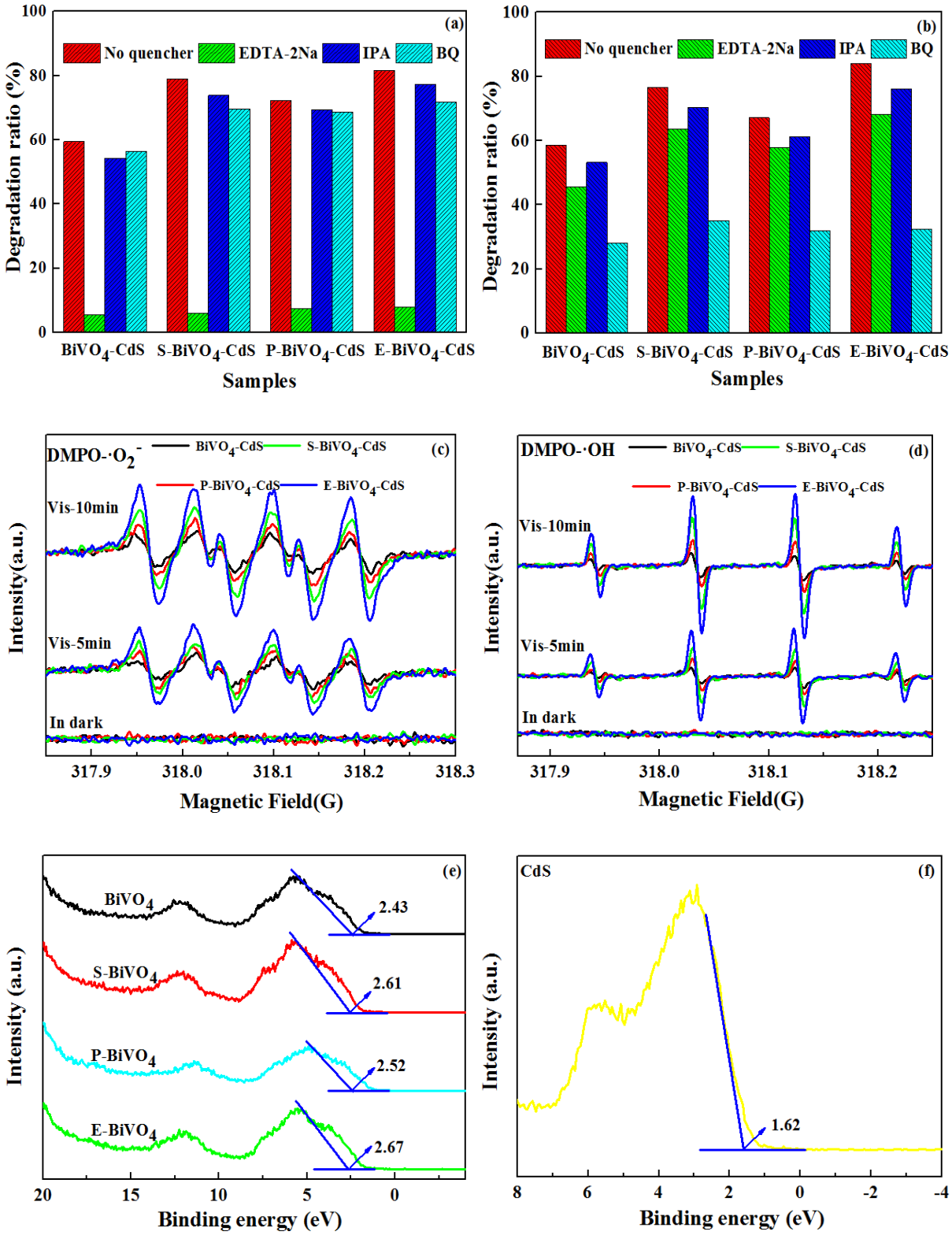

Fig.5. Photocatalytic activities of $BiVO_4$-CdS with the different scavengers for TCH (a) and CIP (b), ESR spectra of DMPO–•O_2^-(c) and DMPO–•OH (d), VB XPS spectra of $BiVO_4$ (e) and CdS (f),

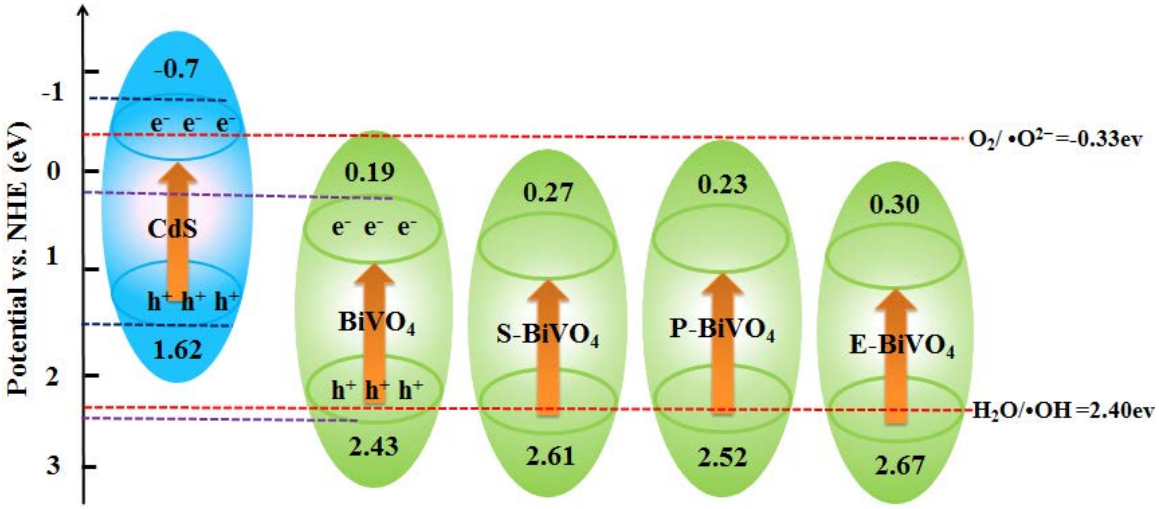

Fig.S5. The band structures of $BiVO_4$ and CdS

In order to deduce the influence of energy-band position difference on performance, the photocatalysis mechanism was investigated. Since the differences in the energy-band positions of all the $BiVO_4$ analogues is very small, the mechanism analysis was carried out by taking $BiVO_4$ as an example. (please check meaning. I'm really not sure) As seen from Fig.6, both $BiVO_4$ and CdS were excited and generated electrons and holes under simulated sunlight irradiation. Furthermore, the electrons and holes will migrate due to the potential difference. If the electron and hole transfer followed the type Ⅱ heterojunction, the electrons and holes will accumulate in the CB of $BiVO_4$ and VB of CdS,. However, the electron in the CB of $BiVO_4$ cannot produce $•O_2^-$(O_2/$•O_2^-$, -0.33 eV vs. NHE), and the hole in the VB of CdS cannot reduce H_2O to •OH (H_2O /•OH, 2.40 eV vs. NHE), which is contrary to the results of the trapping experiments and ESR analyses [38]. Therefore, a more reasonable electronic transmission mechanism Z-scheme heterojunction is proposed; the electron in the CB of $BiVO_4$ can be quickly transferred to the VB of CdS. The holes in the VB of $BiVO_4$ and electrons in the CB of CdS can easily produce •OH and $•O_2^-$ in the photodegradation process. Furthermore, the values of VB and CB in $BiVO_4$ increase in the order: $BiVO_4$ < P-$BiVO_4$< S-$BiVO_4$ < E-$BiVO_4$ (Fig.4f), meaning that E-$BiVO_4$ can generate more •OH and shows the highest electron and hole-separation efficiency. This can be ascribed to the fact that E-$BiVO_4$ and CdS have the

smallest potential difference and E-$BiVO_4$ retains a higher redox potential, which is consistent with the results of the ESR and photoelectrochemical analyses. The results of the mechanism study confirm that the surfactant affects the structure and morphology of $BiVO_4$, which then changes the VB and CB positions of $BiVO_4$, so that they finally better match those of CdS to improve photocatalytic performance.

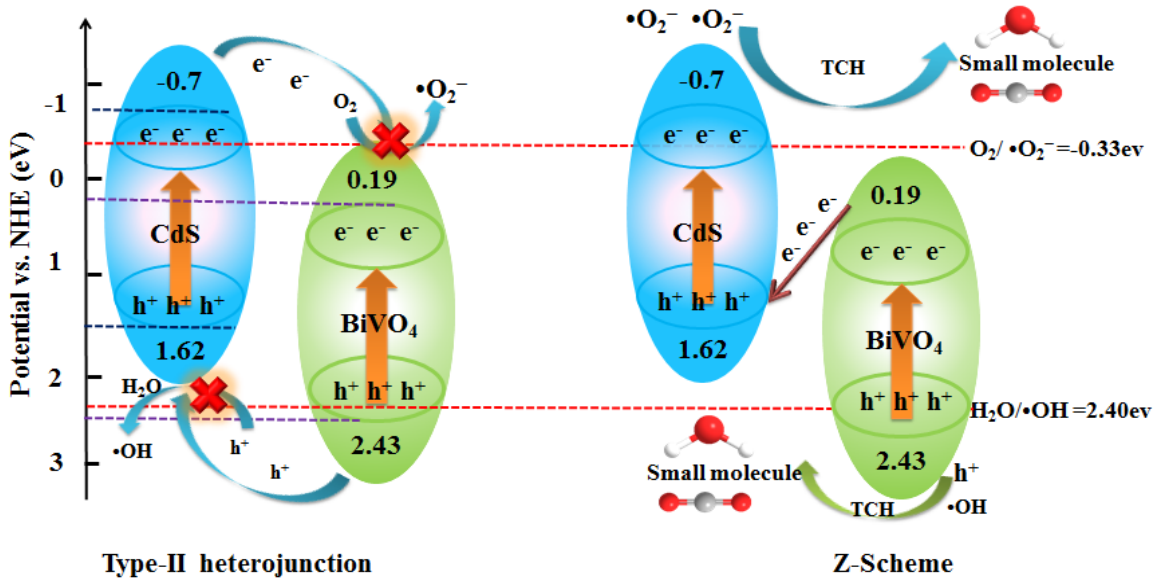

Fig.6. The proposed photocatalysis mechanism for $BiVO_4$-CdS

3.5 Photostability

The stability of the photocatalyst is another vital consideration for practical photocatalytic applications. Repetitive photocatalytic experiments were therefore carried out and the results are demonstrated in Fig.S6. It is clear that no significant reduction in the photocatalytic performance of all $BiVO_4$-CdS against TCH and CIP is observed after three cycles, suggesting that the $BiVO_4$-CdS photocatalyst is highly stable. In addition, the XPS patterns of the recycled $BiVO_4$-CdS display no obvious differences as compared with the fresh sample (Fig.S7-8), suggesting that the chemical status and chemical composition did not changed before and after the reaction. Therefore, the high stability of $BiVO_4$-CdS can provide a basis for practical photocatalytic applications.

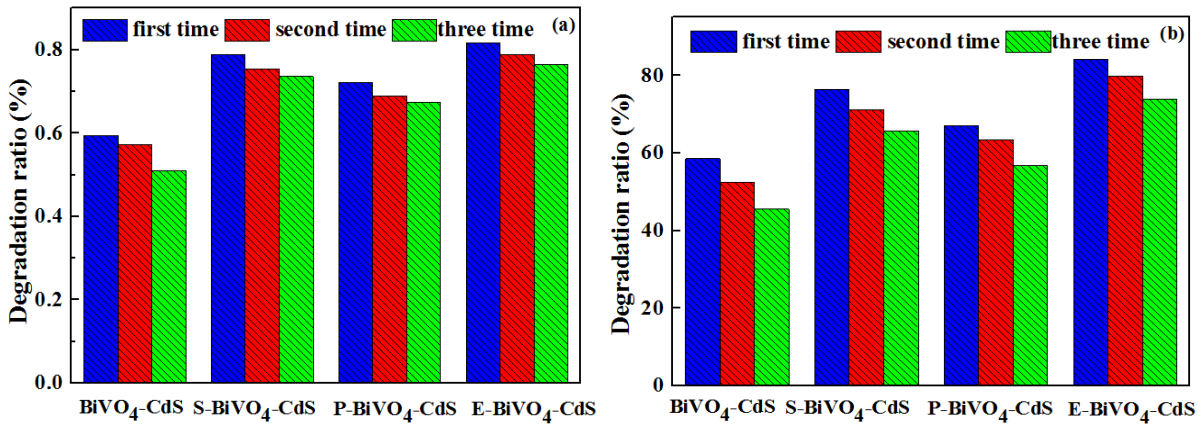

Fig.S6. Repetitive photocatalytic degradation of TCH (a) and CIP (b)

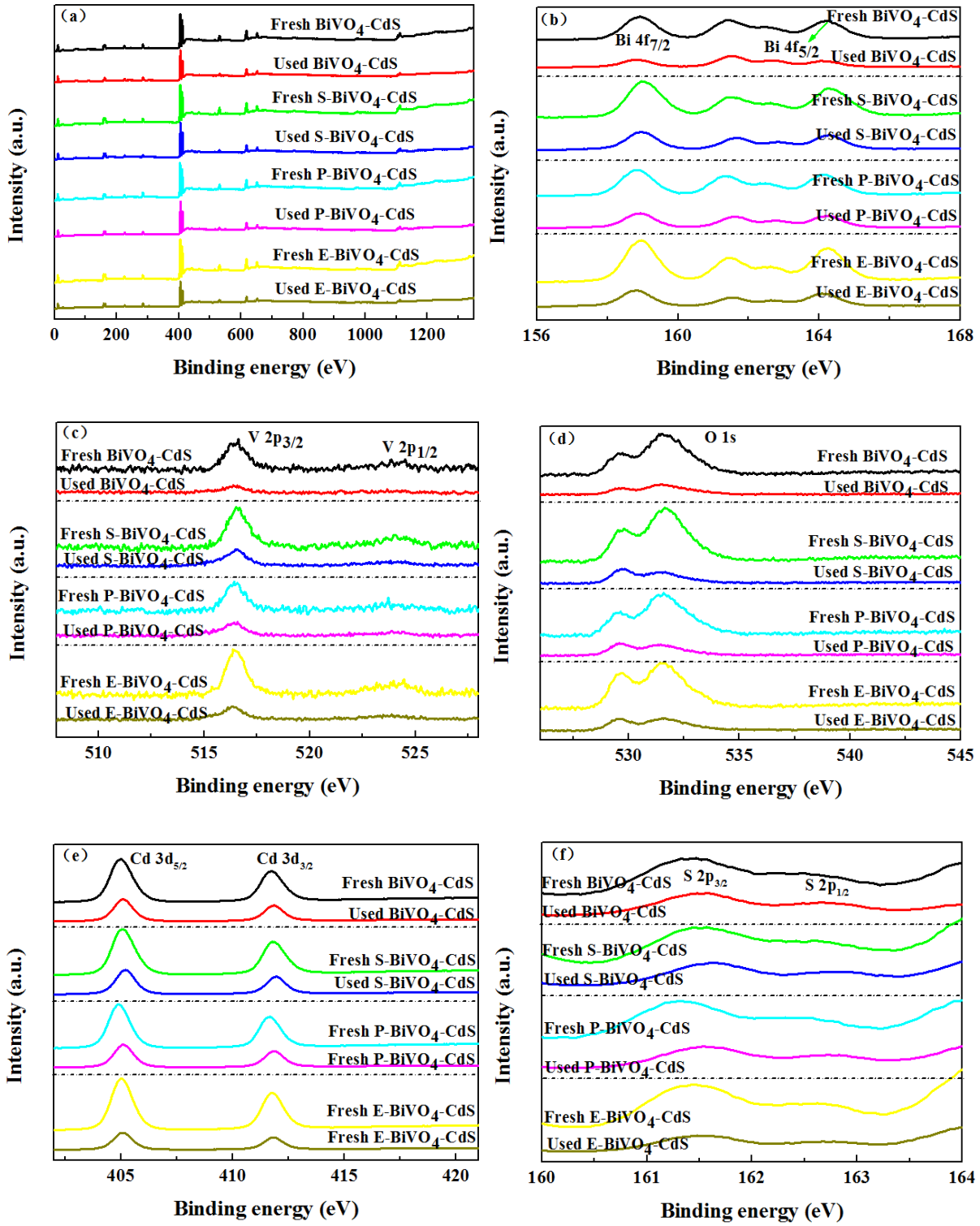

Fig.S7 XPS patterns of $BiVO_4$-CdS before and after three TCH photodegradation runs

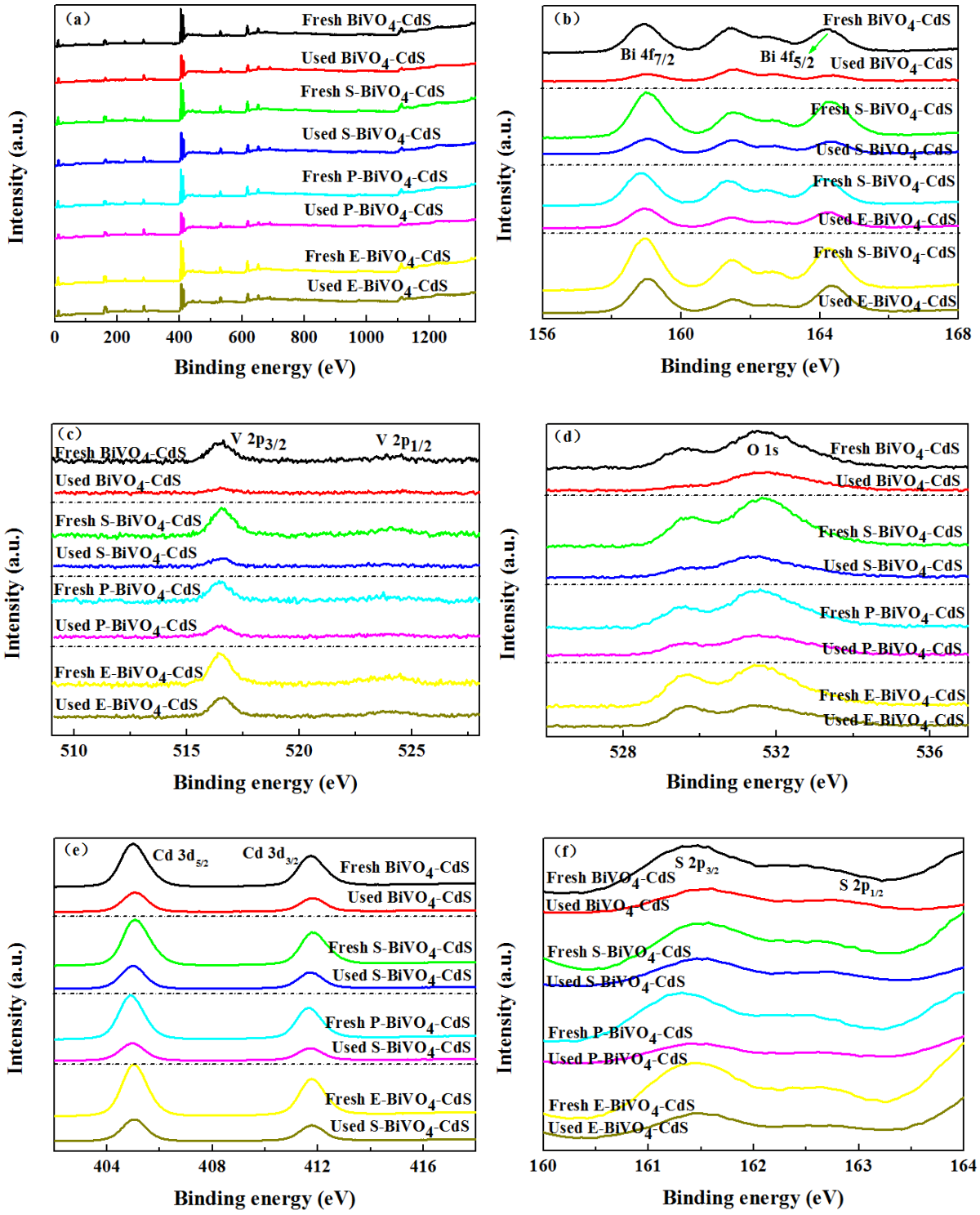

Fig.S8 XPS patterns of $BiVO_4$-CdS before and after three CIP photodegradation runs

4. Conclusions

In summary, $BiVO_4$ analogues with different morphologies have been synthesized using a microwave-assisted method in the presence of surfactants. $BiVO_4$-CdS analogues were then prepared using the chemical-bath-deposition method. The surfactant enhanced the photocatalytic performance of $BiVO_4$ in the order: EDTA>SDBS>PVP>no surfactant, which may be due to the fact that the surfactants changed the morphology of $BiVO_4$, leading to changes in energy-band position and improved separation efficiency of electrons and holes. Moreover, $BiVO_4$-CdS exhibited higher photocatalytic efficiency than $BiVO_4$, which can be ascribed to the fact that the Z-scheme system improves the separation efficiency of electrons and holes. This work provides a fast and efficient way to synthesize Z-scheme photocatalysts of $BiVO_4$-CdS for the photodegradation of TCH and CIP, and also stimulates interest in utilizing surfactants to prepare special morphology nanomaterials with high photocatalytic performance.

Acknowledgments

This work was supported financially by funding from the National Natural Science Foundation of China (21868034), International Science and Technology Cooperation Program of Shihezi University (GJHZ201601) and the University of Turin (Ricerca locale 2018).

Reference

[1] C. Zhou, S. Wang, Z. Zhao, Z. Shi, S. Yan, Z. Zou, Adv. Funct. Mater. 28 (2018) 1801214.

[2] Y. Xue, Z. Wu, X. He, Q. Li, X. Yang, L. Li, J. Colloid Interface Sci. 548 (2019) 292-302.

[3] M. Wang, J. Han, C. Lv, Y. Zhang, M. You, T. Liu, T. Zhu, J. Alloys Compd. 753 (2018) 465-474.

[4] A. Malathi, J. Madhavan, M. Ashokkumar, P. Arunachalam, Appl. Catal., A 555 (2018) 47-74.

[5] Microwave Chemistry Ed. Cravotto, G. and Carnaroglio, D.; 2017 De Gruyter (Berlin, Germany), ISBN 978-3-11-047993-5.

[6] X. Chen, D. Liu, Z. Wu, G. Cravotto, Z. Wu, B. C. Ye, Catal. Commun. 104 (2018) 96-100.

[7] D. Vidyasagar, S. G. Ghugal, A. Kulkarni, A. G. Shende, S. S. Umare, R. Sasikala, New J. Chem. 42 (2018) 6322-6331.

[8] Y. Wang, F. Liu, Y. Hua, C. Wang, X. Zhao, X. Liu, H. Li, J. Colloid Interface Sci. 483 (2016) 307-313.

[9] S. Liu, H. Tang, H. Zhou, G. Dai, W. Wang, Appl. Surf. Sci. 391 (2017) 542-547.

[10] Z. Sun, Z. Yu, Y. Liu, C. Shi, M. Zhu, A. Wang, J. Colloid Interface Sci. 533 (2019) 251-258.

[11] Z. H. Wei, Y. F. Wang, Y. Y. Li, L. Zhang, H. C. Yao, Z. J. Li, J. CO_2 Util. 28 (2018) 15-25.

[12] L. Ye, L. Li, L. Guo, J. Fang, H. Zhao, Y. Jiang, Mater. Lett. 211 (2018) 171-174.

[13] G. Zhao, W. Liu, Y. Hao, Z. Zhang, Q. Li, S. Zang, Dalton Transactions 47 (2018) 1325-1336.

[14] F. Q. Zhou, J. C. Fan, Q. J. Xu, Y. L. Min, Appl. Catal., B 201 (2017) 77-83.

[15] N. C. S. Selvam, Y. G. Kim, D. J. Kim, W. H. Hong, W. Kim, S. H. Park, W. K. Jo, Sci. Total Environ. 635 (2018) 741-749.

[16] Z. H. Wei, Y. F. Wang, Y. Y. Li, L. Zhang, H. C. Yao, Z. J. Li, J. CO_2 Util. 28 (2018) 15-25.

[17] Y. Ming, F. Zhu, G. Wei, S. Lin, W. Shi, Y. Hua, RSC Adv. 6(66) (2016) 10.1039.C6RA07589D.

[18] L. Li, J. Wu, B. Liu, X. Liu, C. Li, Y. Gong, L. Pan, Catal. Today 315 (2018) 110-116.

[19] X. Han, Y. Wei, J. Su, Y. Zhao, ACS Sustain. Chem. Eng. 6 (11) (2018) 14695–14703.

[20] C. Bie, J. Fu, B. Cheng, L. Zhang, Appl. Surf. Sci. 462 (2018) 606-614.

[21] J. Yang, Q. Shi, R. Zhang, M. Xie, X. Jiang, F. Wang, W. Han, Carbon 138 (2018) 118-124.

[22] Y. Xue, Z. Wu, X. He, X. Yang, X. Chen, Z. Gao, Nanomaterials 9 (2019) 222.

[23] S. Liu, H. Tang, H. Zhou, G. Dai, W. Wang, Appl. Surf. Sci.391 (2017) 542-547.

[24] H. B. Li, J. Zhang, G. Y. Huang, S. H. Fu, M. A. Chao, B. Y. Wang, H. W. Liao, Trans. Nonferrous Met. Soc. China 27 (2017) 868-875.

[25] W. Ma, Z. Li, W. Liu, Ceram. Int., 41, (2015) 4340-4347.

[26] Y. Xue, C. Du, Z. Wu, L. Zhang, New J. Chem. 42 (2018) 16493-16502.

[27] J. Zhan, B. Geng, K. Wu, G. Xu, L. Wang, R. Guo, M. Wu, Carbon 130 (2018) 153-163.

[28] R. Bhosale, S. Jain, C. P. Vinod, S. Kumar, S. Ogale, ACS Appl. Mater. Interfaces 11(6) (2019) 6174-6183.

[29] L. Di, H. Yang, T. Xian, X. Liu, X. Chen, Nanomaterials 9 (2019) 399.

[30] C. Li, H. Che, C. Liu, G. Che, P. A. Charpentier, W. Z. Xu, L. Liu, J. Taiwan Inst. Chem. Eng. 95 (2019) 669-681.

[31] J. Xia, J. Di, H. Li, H. Xu, H. Li, S. Guo, Appl. Catal., B 181 (2016) 260-269.

[32] W. Zhao, Y. Feng, H. Huang, P. Zhou, J. Li, L. Zhang, D. Y. Leung, Appl. Catal., B 245, (2019) 448-458.

[33] C. Suwanchawalit, S. Buddee, S. Wongnawa, J. Environ. Sci. 55 (2017) 257-265.

[34] Y. Liu, J. Kong, J. Yuan, W. Zhao, X. Zhu, C. Sun, J. Xie, Chem. Eng. J. 331 (2018) 242-254.

[35] J. Xia, J. Di, H. Li, H. Xu, H. Li, S. Guo, Appl. Catal., B 181 (2016) 260-269.

[36] J. Li, W. Zhang, M. Ran, Y. Sun, H. Huang, F. Dong, Appl. Catal., B 243, (2019) 313-321.

[37] F. Wang, Y. Wu, Y. Wang, J. Li, X. Jin, Q. Zhang, G. Liu, Chem. Eng. J. 356 (2019) 857-868.

[38] W. Wang, P. Xu, M. Chen, G. Zeng, C. Zhang, C. Zhou, L. Hu, ACS Sustain. Chem. Eng. 6(11) (2018) 15503-15516.